Competing magnetic and structural states in multiferroic YMn_2O_5 at high pressure

D. P. Kozlenko,[1] N. T. Dang,[2] S. E. Kichanov,[1] E. V. Lukin,[1] A. M. Pashayev,[3] A. I. Mammadov,[4] S. H. Jabarov,[4,5] L. S. Dubrovinsky,[5] H.-P. Liermann,[6] W. Morgenroth,[7] R. Z. Mehdiyeva,[4] V. G. Smotrakov,[8] and B. N. Savenko[1]

[1]*Frank Laboratory of Neutron Physics, Joint Institute for Nuclear Research, 141980 Dubna, Russia*
[2]*Institute of Research and Development, Duy Tan University, 550000 Da Nang, Viet Nam*
[3]*National Aviation Academy, AZ1045, Baku, Azerbaijan*
[4]*Laboratory of Non-Standard Control and Diagnostics, Institute of Physics, ANAS, AZ-1143, Baku, Azerbaijan*
[5]*Bayerisches Geoinstitut, Universität Bayreuth, D-95440 Bayreuth, Germany*
[6]*Photon Sciences, Deutsches Elektronen Synchrotron, D-22607 Hamburg, Germany*
[7]*Institute of Geosciences, University of Frankfurt, D-60438 Frankfurt, Germany*
[8]*Physics Research Institute, Southern Federal University, 344090, Rostov-on-Don, Russia*

(Received 20 May 2015; revised manuscript received 29 July 2015; published 12 October 2015)

The magnetic, structural, and vibrational properties of YMn_2O_5 multiferroic have been studied by means of neutron, x-ray powder diffraction, and Raman spectroscopy at pressures up to 6 and 30 GPa, respectively. Application of high pressure, $P > 1$ GPa, leads to a gradual suppression of the commensurate and incommensurate antiferromagnetic (AFM) phases with a propagation vector $q = (1/2,0,q_z \sim 1/4)$ and appearance of the commensurate AFM phase with $q = (1/2,0,1/2)$. This observation is sharply contrasting to general trend towards stabilization of commensurate AFM phase with $q = (1/2,0,1/4)$ found in other RMn_2O_5 compounds upon lattice compression. At $P \sim 16$ GPa a structural phase transformation accompanied by anomalies in lattice compression and pressure behavior of vibrational modes was observed. The comparative analysis of high-pressure and R-cation radius variation effects clarified a role of particular magnetic interactions in the formation of the magnetic states of RMn_2O_5 compounds.

DOI: 10.1103/PhysRevB.92.134409 PACS number(s): 75.85.+t, 75.25.−j, 61.50.Ks, 78.30.−j

I. INTRODUCTION

The multiferroic materials, exhibiting simultaneously ferroelectric and magnetic orders, recently have become a subject of extensive scientific research. A coexistence of magnetic order and ferroelectric polarization in multiferroics gives rise to challenging physical phenomena such as magnetoelectric effects, generation of electromagnons, etc., and also provides a route for a development of alternative electronic devices with a possibility of magnetic properties control by electric field and vice versa [1–3].

Generally, two types of multiferroic materials can be distinguished. The first one, "proper" multiferroics like $BiFeO_3$ and hexagonal $RMnO_3$ (R—rare-earth elements), is characterized by ferroelectric transition temperatures significantly exceeding magnetic ordering ones and relatively weak coupling of relevant order parameters [1,2]. The second type, "improper" multiferroics, was discovered more recently and its characteristic feature is occurrence of ferroelectricity due to lattice inversion symmetry breaking by modulated magnetic order. The typical representatives of improper multiferroics are orthorhombic $RMnO_3$, RMn_2O_5 (R = Tb, Ho, Dy, Y, and Bi), and $RbFe(MoO_4)_2$; they exhibit a pronounced magnetoelectric coupling and close ferroelectric transition and magnetic ordering temperatures [3–5].

The RMn_2O_5 compounds are of particular interest since they demonstrate colossal magnetoelectric effects and a complex sequence of magnetic phase transformations, tuning the ferroelectric polarization features [4,6–10]. These materials crystallize in the orthorhombic crystal structure of *Pbam* symmetry which consists of edge-shared chains of $Mn^{4+}O_6$ octahedra along the c axis linked by $Mn^{3+}O_5$ pyramids [11,12]. Below the Néel temperature $T_N \approx 45$ K the antiferromagnetic (AFM) order with a propagation vector $q = (q_x,0,q_z)$ is established, whose components change subsequently on cooling from initially incommensurate to commensurate at $T_{C1} \approx 40$ K and back to incommensurate at $T_{C2} \approx 20$ K. In the commensurate AFM phase, the values $q_x \sim 1/2$ and $q_z \sim 1/4$ were found for almost all of the R elements except for Bi, having $q_z = 1/2$ and Gd, having $q_z = 0$ [9,13]. The spontaneous ferroelectric polarization oriented along the b axis arises below T_{C1}, and it exhibits a rapid drop below T_{C2} [6–10].

The nature of the magnetoelectric coupling in RMn_2O_5 compounds, arising from the complex interplay of magnetic frustration due to competing superexchange interactions between Mn^{3+}, Mn^{4+}, and R^{3+} ions, and spin, lattice, and orbital degrees of freedom, is still extensively debated. The possible scenarios involve the magnetoelastic coupling model [8] based on symmetric exchange interactions and providing polarization proportional to a scalar product of neighboring spins, $P \sim (S_i S_j)$ and spin current model [14,15] based on antisymmetric exchange Dzyaloshinskii-Moriya interactions, resulting in polarization proportional to a vector product of neighboring spins, $P \sim [S_i \times S_j]$.

An important insight into the relationship between the competing factors above and their particular role in formation of magnetoelectric properties of RMn_2O_5 compounds can be given by high-pressure studies, exploring response of physical properties on reduction of interatomic distances, mediating relevant interactions. Recently it was found that upon application of high-pressure RMn_2O_5 compounds follow a general trend towards stabilization of the commensurate AFM ground state with $q = (1/2,0,1/4)$ [16,17]. In the present paper we show that YMn_2O_5 demonstrates sharply contrasting behavior. In this compound, lattice compression

leads to stabilization of the alternative AFM ground state with $q = (1/2,0,1/2)$, similar to one formed in $BiMn_2O_5$ on an expanded lattice due to *R*-cation substitution. A structural phase transformation in YMn_2O_5 at extended pressures was also evidenced.

II. EXPERIMENT

YMn_2O_5 powdered sample was obtained from single crystals grown using the PbO-PbF_2-B_2O_3 flux method.

Angle-dispersive x-ray powder diffraction patterns at high pressures up to 30 GPa and ambient temperature were measured at the Extreme Conditions Beamline [18] (ECB) P02.2 at the third-generation synchrotron radiation source PETRA III located at the Deutsches Elektronen Synchrotron (DESY) Hamburg, Germany. The diffraction images were collected with the wavelength $\lambda = 0.29118$ Å on the amorphous silicon flat panel detector bonded to a ScI scintillator (XRD 1621) from PerkinElmer and located at a distance of 402.33 mm from the sample. The two-dimensional x-ray diffraction (XRD) images were converted to one-dimensional diffraction patterns using the FIT2D program [19].

Raman spectra at ambient temperature and pressures up to 30 GPa were collected using a LabRam spectrometer (NeHe excitation laser) with wavelength of 632.8 nm, 1800 grating, confocal hole of 1100 μm, and a 50× objective. The BX90 type diamond anvil cell [20] was used for the x-ray diffraction and Raman experiments. The sample was loaded into the hole of the 150-μm diameter made in the Re gasket indented to about 30 μm thickness. Diamonds with culets of 300 μm were used. Neon gas loaded under pressure of ~0.15 GPa was used as a pressure transmitting medium. The pressure was determined by the ruby fluorescence technique [21].

Neutron powder diffraction measurements at high pressures up to 6.5 GPa were performed at selected temperatures in the range 10−290 K with the DN-12 diffractometer [22] at the IBR-2 high-flux pulsed reactor (FLNP JINR, Dubna, Russia). The sample with a volume of about 2 mm^3 was loaded into the sapphire anvil high-pressure cell [23]. Several tiny ruby chips were placed at different points of the sample surface and the pressure was determined by a standard ruby fluorescence technique. Measurements of the pressure distribution on the sample yield typical pressure inhomogeneities of ±15%. Diffraction patterns were collected at scattering angle 90° with the resolution $\Delta d/d = 0.015$. Experimental data of the x-ray and neutron powder diffraction experiments were analyzed by the Rietveld method using the FULLPROF [24] program.

III. RESULTS

A. X-ray diffraction

X-ray diffraction patterns (XRD) of YMn_2O_5 measured at selected pressures and ambient temperature are shown in Fig. 1. At moderate pressures, they correspond to the orthorhombic crystal structure of *Pbam* symmetry. The values of lattice parameters determined at ambient conditions are consistent with previous studies [8–11]. The lattice compression of YMn_2O_5 is markedly anisotropic with the most compressible *a* lattice parameter and weakly compressible *b* and

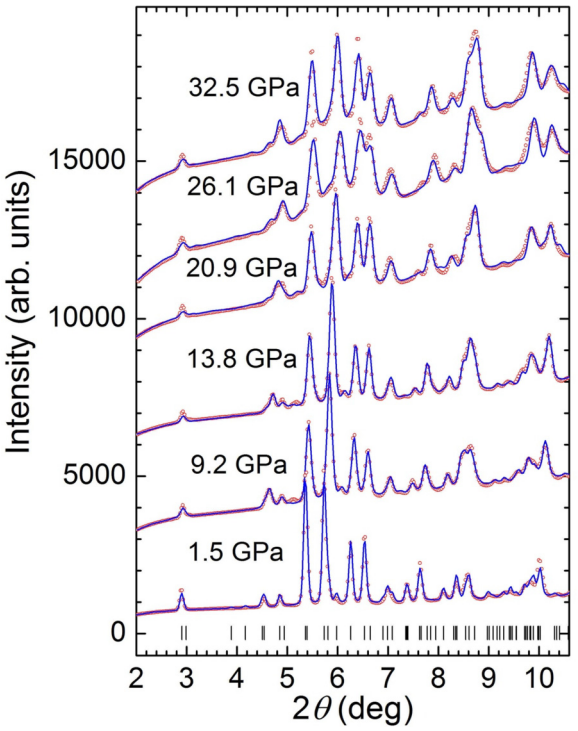

FIG. 1. (Color online) X-ray diffraction patterns of YMn_2O_5 measured at selected pressures and ambient temperature, and refined by the Rietveld method. Experimental points and calculated profiles are shown. Tick marks at the bottom represent the calculated positions of diffraction peaks.

c lattice parameters. The relevant average compressibilities $[k_i = -(1/a_{i0})(da_i/dP)_T]$ are $k_a = 0.0028$, $k_b = 0.0009$, and $k_c = 0.0007$ GPa^{-1}, respectively. At $P \approx 16$ GPa, anomalies in pressure behavior of lattice parameters were observed, evidencing a structural phase transformation (Fig. 2). An absence of the extra peaks and qualitatively similar character of XRD data over the whole studied pressure range implies either isostructural phase transformation or phase transition caused by orientational rearrangement of the MnO_6 octahedra

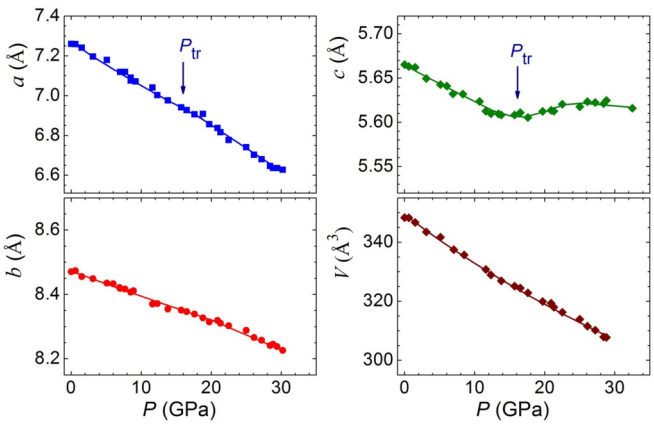

FIG. 2. (Color online) Lattice parameters and unit cell volume of YMn_2O_5 as functions of pressure and their interpolation based on the Birch-Murnaghan equation of state.

and MnO_5 pyramids within the unit cell. As a reasonable approach, the orthorhombic *Pbam* structural model for the high-pressure phase was used and satisfactory fitting of the experimental data was achieved. The phase transformation results in enlargement of the *c* lattice parameter compensated by additional shrinking of the *a* and *b* parameters, so the unit cell volume does not exhibit any pronounced peculiarities at the transformation pressure (Fig. 2). Similar features were also recently found in the lattice compression of the relevant $BiMn_2O_5$ compound, but at noticeably lower pressure, $P \sim 10$ GPa [25].

The volume compressibility data of YMn_2O_5 (Fig. 2) were fitted by the third-order Birch-Murnaghan equation of state [26]:

$$P = \frac{3}{2}B_0(x^{-7/3} - x^{-5/3})\left[1 + \frac{3}{4}(B' - 4)(x^{-2/3} - 1)\right],$$

where $x = V/V_0$ is the relative volume change; V_0 is the unit cell volume at ambient pressure; and B_0, B' are the bulk modulus $[B_0 = -V(dP/dV)_T]$ and its pressure derivative $[B' = (dB_0/dP)_T]$. Despite changes in particular lattice compressibilities due to the phase transformation (Fig. 2), volume

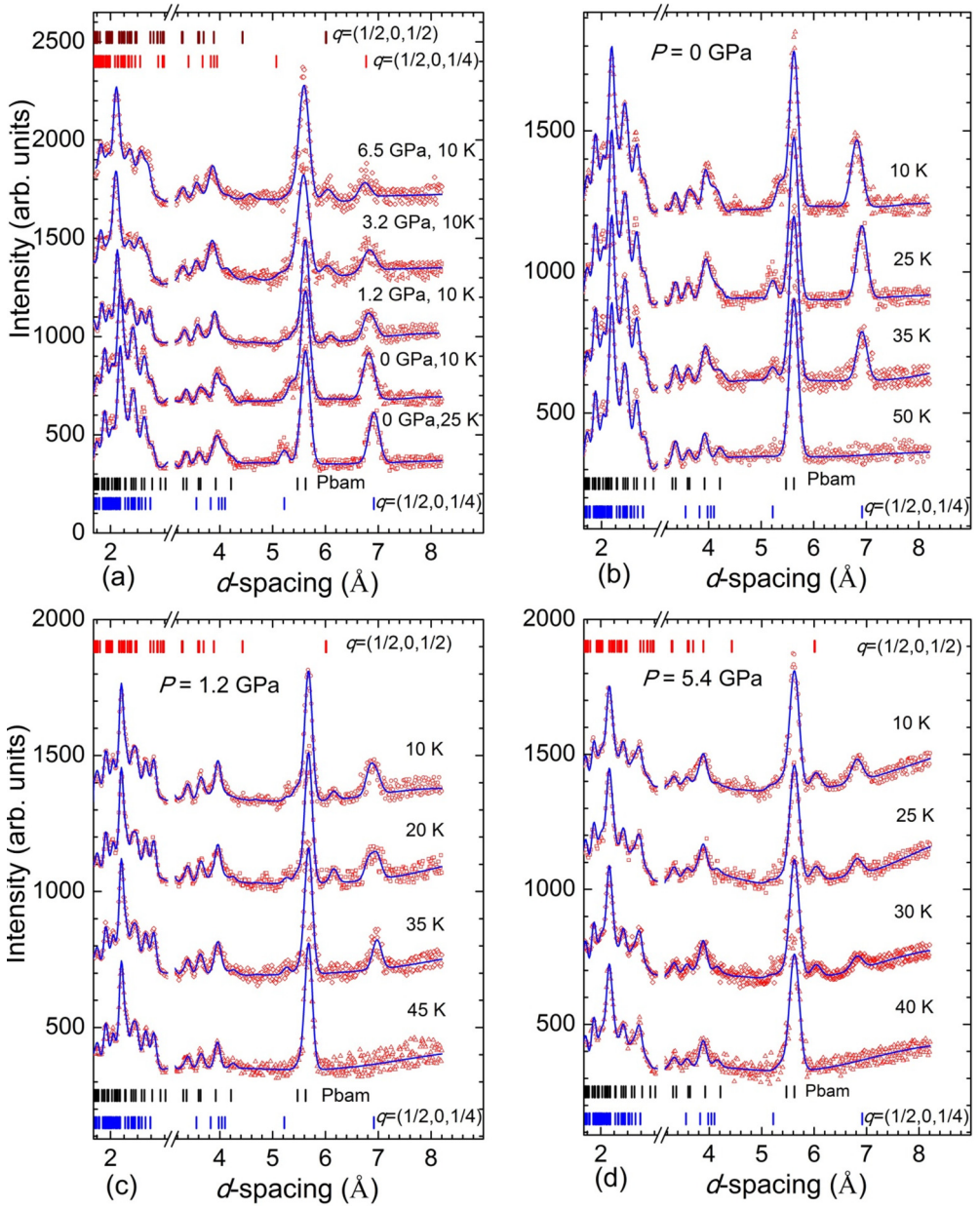

FIG. 3. (Color online) Neutron diffraction patterns of YMn_2O_5, measured at selected pressures up to 6.5 GPa and low temperatures (a), pressures 0, 1.2, 5,4 GPa and selected temperatures (b, c, d), and processed by the Rietveld method. The experimental points and calculated profiles are shown. Ticks below represent calculated positions of the nuclear peaks of the orthorhombic *Pbam* phase (upper row) and magnetic peaks of the AFM phase with $q = (1/2\ 0\ 1/4)$. Ticks at the top of the panel (a) represent the calculated positions of the magnetic peaks of the AFM phases with $q_p = (1/2\ 0\ 1/2)$ and $q = (1/2\ 0\ 1/4)$ for $P = 6.5$ GPa and $T = 10$ K. Ticks at the top of the panels (b–d) represent calculated positions of the magnetic peaks of the AFM phase with $q_p = (1/2\ 0\ 1/2)$.

compressibility data of two phases can be fitted with about the same values of bulk modulus and its pressure derivative, $B_0 = 192(5)$ GPa and $B' = 3.0(5)$. This value is larger in comparison with those obtained for $HoMn_2O_5$ (173 GPa) and $BiMn_2O_5$ (145 and 167 GPa for ambient-pressure and high-pressure phases) [27,25].

B. Neutron diffraction

Neutron diffraction patterns of YMn_2O_5, measured at selected pressures and temperatures, are shown in Fig. 3. The characteristic values of R factors were $R_p = 4.2$, $R_{wp} = 5.7\%$ for 0 GPa, $R_p = 6.8$, $R_{wp} = 9.6\%$ for 1.2 GPa, $R_p = 8.1$, $R_{wp} = 10.6\%$ for 6.5 GPa, $T = 10$ K. An appearance of magnetic peaks was observed below $T_N \approx 45$ K (Figs. 3 and 4), whose positions at $d_{hkl} = 6.90$, 5.20, and 3.98 Å for $T < T_{C1} = 40$ K correspond to formation of the commensurate AFM order with a propagation vector $q = (1/2\ 0\ 1/4)$. Below $T_{C2} \approx 20$ K, the magnetic order becomes incommensurate with the $q = (0.49\ 0\ 0.29)$, as detected from the magnetic peaks positions shift.

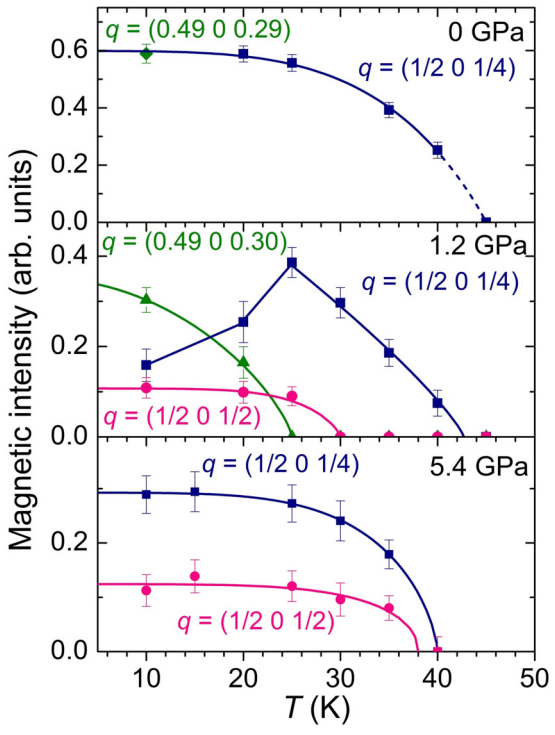

FIG. 4. (Color online) Temperature dependences of the integrated intensity of the magnetic peak $(1-q_x, -1, -q_z)/(1-q_x, 1, -q_z)/(\pm q_x, 1, \pm q_z)$ for the commensurate and incommensurate AFM phases with $q = (\sim 1/2, 0, \sim 1/4)$ and the integrated intensity of the magnetic peak $(-q_x, 1, 1-q_z)$ for the commensurate AFM phase with $q_p = (1/2\ 0\ 1/2)$ at selected pressures. The solid lines represent interpolations by functions $I = I_0[1-(T/T_N)^{\alpha}]^{2\beta}$. The values of the q_x and q_z components of the propagation vector for the suppressed incommensurate AFM phase at $T = 10$ K are also given. The dashed line in the top panel represents the expected temperature range of the existence of another incommensurate AFM phase formed in the vicinity of T_N, not studied in detail in the present paper.

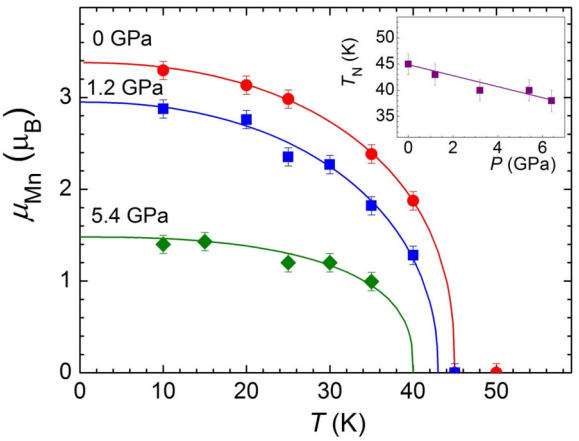

FIG. 5. (Color online) Temperature dependencies of the average ordered Mn^{3+}/Mn^{4+} magnetic moment at selected pressures. The solid lines represent interpolations by functions $\mu = \mu_0[1-(T/T_N)^{\alpha}]^{\beta}$. Inset: pressure dependence of the Néel temperature and its linear interpolation.

Due to the small temperature interval of the existence of the incommensurate AFM phase in the vicinity of T_N, in high-pressure experiments we concentrated on the intermediate- and low-temperature AFM phases only. At pressure $P = 1.2$ GPa two effects were observed (Fig. 3). The first is an additional broadening of the magnetic peak $(1-q_x, -1, -q_z)/(1-q_x, 1, -q_z)/(\pm q_x, 1, \pm q_z)$ located at $d_{hkl} = 6.90$ Å at temperatures below 20 K, indicating a coexistence of the incommensurate and commensurate AFM phases (Fig. 4). The second is an appearance of an extra magnetic peak at $d_{hkl} = 6.08$ Å and redistribution of magnetic intensity in the d-spacing range 3.60−4.15 Å, evidencing a formation of a new magnetic phase (Figs. 3 and 4). At pressures above 3.2 GPa the incommensurate AFM phase was fully suppressed. In addition, a gradual suppression of the magnetic peaks corresponding to the commensurate AFM phase with a propagation vector $q = (1/2\ 0\ 1/4)$ was observed. The average ordered magnetic moment of the Mn^{3+}/Mn^{4+} ions at $T = 10$ K is reduced about two times over the 0−6.5 GPa pressure range from 3.30(5) to $1.40(7)\mu_B$. From the temperature dependences of the average ordered magnetic moments, a decrease of the Néel temperature with a pressure coefficient $dT_N dP = -1.1$ K/GPa is established (Fig. 5). At the same time, a progressive growth of the intensity of the magnetic peak located at $d_{hkl} = 6.00$ Å, corresponding to a newly appeared magnetic phase, occurs upon compression (Fig. 3). The data analysis of the magnetic contribution to diffraction patterns has shown that the pressure-induced magnetic phase has the AFM order with a propagation vector $q_p = (1/2\ 0\ 1/2)$. The Néel temperature, estimated from the temperature evolution of the magnetic peak $(-q_x, 1, 1-q_z)$ intensity (Fig. 4), reaches the value $T_{Np} = 38(3)$ K at pressure 5.4 GPa. The gradually suppressed AFM phase with the propagation vector $q = (1/2\ 0\ 1/4)$ and the pressure-induced AFM phase with the propagation vector $q_p = (1/2\ 0\ 1/2)$ coexist in the temperature range below T_{Np}. The average ordered magnetic moment of Mn^{3+}/Mn^{4+} ions in the latter phase reaches the value $\mu_p = 0.70(5)\mu_B$ at $P = 6.5$ GPa and $T = 10$ K. Comparing

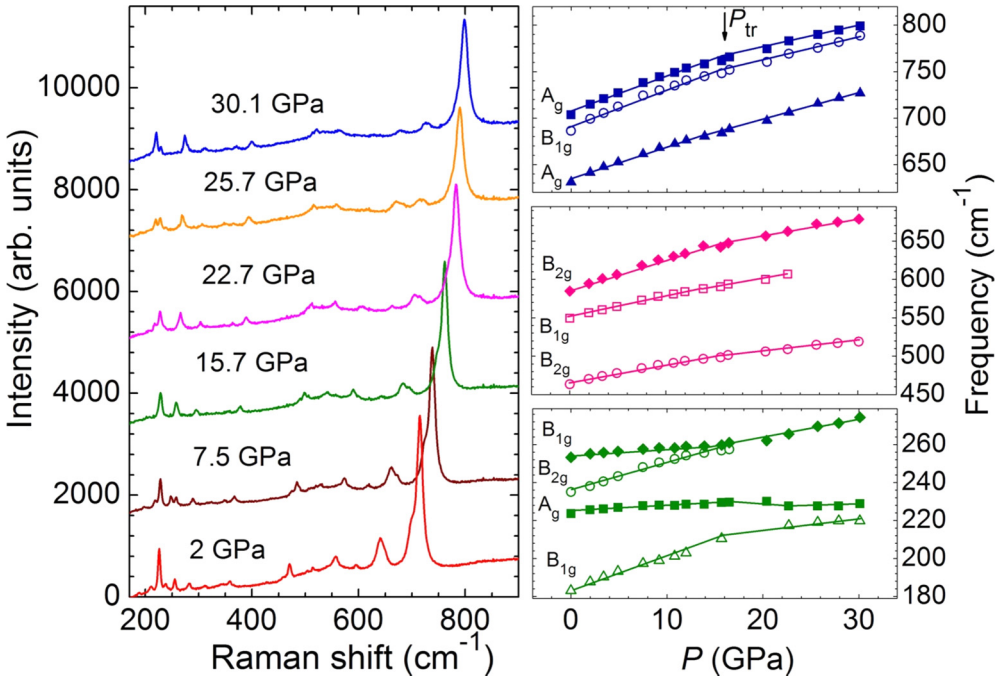

FIG. 6. (Color online) Raman spectra of YMn_2O_5 at selected pressures (left). Pressure dependencies of the selected vibrational modes frequencies and their linear interpolation (right). The error bars are within the symbol sizes.

this value to one corresponding to the initial commensurate AFM phase, one may evaluate a volume ratio of the competing AFM phases with propagation vectors $q = (1/2\ 0\ 1/4)$ and $q_p = (1/2\ 0\ 1/2)$ as 34% : 66%, respectively.

C. Raman spectroscopy

The Raman spectra of YMn_2O_5 measured at selected pressures and ambient temperature are shown in Fig. 6. At moderate pressures, 13 lines at 183, 206, 223, 235, 253, 278, 354, 463, 549, 586, 631, 686, and 703 cm^{-1} are detected. For the orthorhombic *Pbam* symmetry, the group theory predicts 48 Raman active modes, $\Gamma_{Ram} = 13A_g + 13B_{1g} + 11B_{2g} + 11B_{3g}$ [28]. According to a previous study of $HoMn_2O_5$ and $TbMn_2O_5$ at ambient pressure [29], the observed lines can be tentatively assigned to the modes of A_g(206, 223, 354, 631, 703 cm^{-1}), B_{1g}(183, 253, 549, 686 cm^{-1}), B_{2g}(235, 463, 586 cm^{-1}), and B_{3g}(278 cm^{-1}) symmetry, respectively. A comparison with relevant orthorhombic and hexagonal $RMnO_3$ compounds [30,31], having octahedral and pentahedral oxygen coordination around Mn atoms, implies that the modes located in the regions 580−710 and 270−560 cm^{-1} involve stretching and bending vibrations of oxygen atoms of Mn-O polyhedra, respectively. The modes located in the 180−270 cm^{-1} most likely correspond to rotational vibrations of Mn-O polyhedra and vibrations involving Y atoms.

At pressures below the phase transformation pressure $P_{tr} =$ 16 GPa, an increase of the observed modes frequencies occurs. The pressure coefficients $k_{vi} = (1/\nu_{i0})d\nu_i/dP$ for modes located in the stretching region are about 0.0059−0.0070 GPa^{-1} and they are larger in comparison with ones located in the bending region, 0.0044−0.0052 GPa^{-1} (Table I). These values are similar to ones found for $HoMn_2O_5$ and smaller in comparison with $BiMn_2O_5$ [27]. Considering the 180−340 cm^{-1} region, the pressure coefficients for the modes B_{1g}, A_g, B_{2g}($\nu_{i0} =$ 183, 206, and 235 cm^{-1}), 0.0069−0.0089 GPa^{-1}, are noticeably larger with respect to those of the modes A_g, B_{1g}($\nu_{i0} =$ 223 and 253 cm^{-1}), 0.0018−0.0019 GPa^{-1}. In rare-earth manganese oxides, lowest-pressure coefficients are characteristic to rotational modes of Mn-O polyhedra. Therefore, one can associate the latter A_g and B_{1g} modes with oxygen rotational vibrations, while the former B_{1g}, A_g, B_{2g} ones—with vibrations involving Mn and O atoms [32,33].

In the vicinity of the transformation pressure $P_{tr} = 16$ GPa, anomalies in the pressure behavior of the majority of

TABLE I. Assignment and pressure coefficients $[(1/\nu_{i0})d\nu_i/dP]$ of Raman modes in the ambient- and high-pressure phases of YMn_2O_5.

		Pressure coefficient (GPa^{-1})	
Mode (cm^{-1})	Assignment	Ambient-pressure phase	High-pressure phase (P>16 GPa)
703.5(0 GPa)	A_g	0.0059	0.0035
686.3(0 GPa)	B_{1g}	0.0066	0.0039
631.0(0 GPa)	A_g	0.0060	0.0045
584.8(0 GPa)	B_{2g}	0.0070	0.0039
549.5(0 GPa)	B_{1g}	0.0052	0.0038
463.3(0 GPa)	B_{2g}	0.0055	0.0028
354.2(0 GPa)	A_g	0.0044	0.0043
278.4(0 GPa)	B_{3g}	0.0047	0.0047
253.3(0 GPa)	B_{1g}	0.0019	0.0039
235.0(0 GPa)	B_{2g}	0.0068	—
223.7(0 GPa)	A_g	0.0018	0.0007
206.1(0 GPa)	A_g	0.0080	—
183.0(0 GPa)	B_{1g}	0.0090	0.0016

vibrational modes are observed, related to reduction of the pressure coefficients (Table I). The $B_{2g}(\nu_{i0} = 235\ \mathrm{cm}^{-1})$ and $B_{1g}(\nu_{i0} = 253\ \mathrm{cm}^{-1})$ modes merge at the transformation point and just one mode appears at $P > P_{tr}$ (Fig. 6). The A_g mode ($\nu_{i0} = 223\ \mathrm{cm}^{-1}$) demonstrates a subtle frequency decrease at P_{tr}, followed by further increase with 2.5 times reduced pressure coefficient. These effects are caused by the rearrangement of Mn-O polyhedral orientation as well as shifts of Y atoms in the unit cell due to the structural phase transformation.

IV. DISCUSSION

The magnetic behavior of YMn_2O_5 under pressure is drastically contrasting with relevant RMn_2O_5 compounds (R = Ho, Tb, Dy) [16,17]. In the latter case, pressure-induced stabilization of the intermediate commensurate AFM state with a propagation vector $q = (1/2\ 0\ 1/4)$, accompanied by a ferroelectric polarization enhancement and a suppression of the incommensurate AFM ground state occurs. In YMn_2O_5, both incommensurate and commensurate AFM states with $q = (\sim 1/2, 0, \sim 1/4)$ are gradually suppressed and AFM commensurate ground state with $q_p = (1/2\ 0\ 1/2)$ appears instead upon lattice compression.

Surprisingly, the magnetic ground state of compressed YMn_2O_5 is similar to one formed in $BiMn_2O_5$ with enlarged lattice due to variation of the R-element ionic radius. The common feature of both compounds is the nonmagnetic nature of R elements, restricting consideration of magnetic interactions to those involving Mn ions only. The $BiMn_2O_5$ compound, demonstrating only commensurate AFM ground state with $q = (1/2\ 0\ 1/2)$ and no incommensurate phases, is known as an exception from the generalized magnetic behavior of the RMn_2O_5 family [9,34]. The Bi^{3+} has the largest ionic radius (1.31 Å) in comparison with Y (1.16 Å) and characteristic values for R elements (1.16−1.25 Å) [35]. It was assumed that the q_z component of the propagation vector is mediated by the magnetic interactions between Mn^{4+} ions in the octahedral chains formed along the c axis (J_1 and J_2 in Fig. 7), which become weaker in $BiMn_2O_5$ with the largest

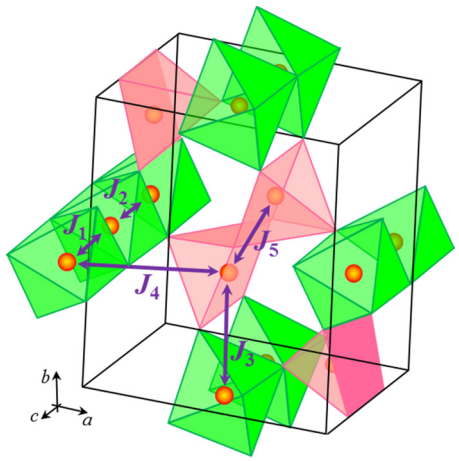

FIG. 7. (Color online) Crystal structure and the nearest-neighbor magnetic interactions in YMn_2O_5. Only the Mn atoms and Mn-O polyhedra are shown.

c-axis lattice parameter and Mn^{4+}-O distances [34]. However, in YMn_2O_5 the c axis demonstrates the weakest compression with respect to a and b axes (Fig. 2) implying that additional driving mechanisms should be involved in the stabilization of the AFM state with $q_p = (1/2\ 0\ 1/2)$. Each of the Mn^{4+} ions is also linked to a couple of Mn^{3+} ions in pyramidal coordination via superexchange interactions J_3, J_4 (Fig. 7). It is reasonable to suggest that the q_z value of the propagation vector in commensurate AFM phases of RMn_2O_5 depend on the ratio of the Mn^{3+}-Mn^{3+}(J_1, J_2) and Mn^{3+}-O^{2-}-Mn^{4+}(J_3, J_4) magnetic interactions strength, which reach a similar proportion in YMn_2O_5 upon compression and in $BiMn_2O_5$ due to lattice enlargement by ionic radius variation, providing similar magnetic states.

In $BiMn_2O_5$, the AFM phase with $q = (1/2\ 0\ 1/2)$ possesses ferroelectric polarization comparable with other RMn_2O_5 compounds [36]. Consequently, the multiferroic character of the commensurate AFM phase with $q_p = (1/2\ 0\ 1/2)$, stabilized in YMn_2O_5 by high pressure, may be expected as well. In the recent study of high-pressure effects on ferroelectric polarization of YMn_2O_5 at moderate pressures up to 1.8 GPa its sign reversal at $P \sim 1$ GPa followed by polarization magnitude enhancement was detected [37]. Such a behavior correlates with the observed suppression of the low-temperature incommensurate AFM phase bearing opposite polarization sign with respect to that expected for commensurate phases, coexisting at high pressure.

V. CONCLUSIONS

The present results demonstrate a pronounced response of the AFM state modulation in YMn_2O_5 with respect to application of high pressure, The initial commensurate and incommensurate magnetic phases with propagation vector $q = (1/2\ 0\ q_z)$, $q_z \sim 1/4$ are gradually suppressed and a commensurate AFM ground state with $q_z \sim 1/2$ is stabilized instead at $P > 1.2$ GPa. This behavior is challenging the general trend towards stabilization of the commensurate antiferromagnetic phase with $q = (1/2\ 0\ 1/4)$ found for RMn_2O_5 compounds at high pressure. Moreover, a similar magnetic state is also realized in RMn_2O_5 for R = Bi due to chemical doping effects accompanied by lattice enlargement. A comparison between these two cases shows that the q_z component of the propagation vector in RMn_2O_5 compounds is controlled not only by a variation of the Mn^{4+}-Mn^{4+} magnetic interactions in octahedral chains, but rather by a delicate balance between these interactions and likely Mn^{4+}-O^{2-}-Mn^{3+} ones with Mn^{3+} ions in pyramidal configuration. Similar to $BiMn_2O_5$, a presence of ferroelectric polarization in the pressure-induced magnetic phase of YMn_2O_5 is expected as well.

At high pressure, $P \sim 16$ GPa, a structural phase transformation in YMn_2O_5 occurs. Modification of lattice parameters, their compression, and anomalies in pressure behavior of the vibrational modes point to rearrangement of Mn-O polyhedra orientations as well as possible shifts of Y atoms in the unit cell. Further experimental studies are required to explore potential multiferroic behavior of this structural phase.

ACKNOWLEDGMENTS

The work has been supported by the Russian Foundation for Basic Research (RFBR) Grant No. 15-02-03248-a and the Vietnam National Foundation for Science and Technology Development (NAFOSTED) under Grant No. 103.02-2014.11. Portions of this research were carried out at the light source PETRA III at DESY, a member of the Helmholtz Association (HGF). Financial support from the Federal Ministry of Education and Research (BMBF), Germany (Projects No. 05K10RFA and No. 05K13RF1) is gratefully acknowledged.

[1] G. A. Smolenskii and I. E. Chupis, Sov. Phys. Usp. **25**, 475 (1982).
[2] M. Fiebig, J. Phys. D **38**, R123 (2005).
[3] T. Kimura, T. Goto, H. Shintani, K. Ishizaka, T. Arima, and Y. Tokura, Nature **426**, 55 (2003).
[4] S.-W. Cheong and M. Mostovoy, Nat. Mater. **6**, 13 (2007).
[5] M. Kenzelmann, G. Lawes, A. B. Harris, G. Gasparovic, C. Broholm, A. P. Ramirez, G. A. Jorge, M. Jaime, S. Park, Q. Huang, A.Ya. Shapiro, and L. A. Demianets, Phys. Rev. Lett. **98**, 267205 (2007).
[6] N. Hur, S. Park, P. A. Sharma, S. Guha, and S.-W. Cheong, Phys. Rev. Lett. **93**, 107207 (2004).
[7] G. R. Blake, L. C. Chapon, P. G. Radaelli, S. Park, N. Hur, S.-W. Cheong, and J. Rodriguez-Carvajal, Phys. Rev. B **71**, 214402 (2005).
[8] L. C. Chapon, P. G. Radaelli, G. R. Blake, S. Park, and S.-W. Cheong, Phys. Rev. Lett. **96**, 097601 (2006).
[9] C. Vecchini, L. C. Chapon, P. J. Brown, T. Chatterji, S. Park, S.-W. Cheong, and P. G. Radaelli, Phys. Rev. B **77**, 134434 (2008).
[10] R. A. de Souza, U. Staub, V. Scagnoli, M. Garganourakis, Y. Bodenthin, S.-W. Huang, M. García-Fernández, S. Ji, S.-H. Lee, S. Park, and S.-W. Cheong, Phys. Rev. B **84**, 104416 (2011).
[11] S. Quezel-Ambrunaz, E. F. Bertaut, and G. Buisson, Comp. Rend. Acad. Sci. Paris **258**, 3025 (1964).
[12] J. A. Alonso, M. T. Casais, M. J. Martínez-Lope, J. L. Martínez, and M. T. Fernández-Díaz, J. Phys.: Condens. Matter **9**, 8515 (1997).
[13] N. Lee, C. Vecchini, Y. J. Choi, L. C. Chapon, A. Bombardi, P.-G. Radaelli, and S.-W. Cheong, Phys. Rev. Lett. **110**, 137203 (2013).
[14] H. Katsura, N. Nagaosa, and A. V. Balatsky, Phys. Rev. Lett. **95**, 057205 (2005).
[15] H. Kimura, Y. Sakamoto, M. Fukunaga, H. Hiraka, and Y. Noda, Phys. Rev. B **87**, 104414 (2013).
[16] C. R. dela Cruz, B. Lorenz, Y. Y. Sun, Y. Wang, S. Park, S.-W. Cheong, M. M. Gospodinov, and C. W. Chu, Phys. Rev. B **76**, 174106 (2007).
[17] H. Kimura, K. Nishihata, Y. Noda, N. Aso, K. Matsubayashi, Y. Uwatoko, and T. Fujiwara, J. Phys. Soc. Jpn. **77**, 063704 (2008).
[18] H.-P. Liermann, W. Morgenroth, A. Ehnes, A. Berghäuser, B. Winkler, H. Franz, and E. Weckert, J. Phys.: Conf. Ser. **215**, 012029 (2010).
[19] A. P. Hammersley, S. O. Svensson, M. Hanfland, A. N. Fitch, and D. Hausermann, High Press. Res. **14**, 235 (1996).
[20] N. A. Dubrovinskaia and L. S. Dubrovinsky, Rev. Sci. Instrum. **74**, 3433 (2003).
[21] H. K. Mao, P. M. Bell, J. W. Shaner, and D. J. Steinberg, J. Appl. Phys. **49**, 3276 (1978).
[22] V. L. Aksenov, A. M. Balagurov, V. P. Glazkov, D. P. Kozlenko, I. V. Naumov, B. N. Savenko, D. V. Sheptyakov, V. A. Somenkov, A. P. Bulkin, V. A. Kudryashev, and V. A. Trounov, Physica B **265**, 258 (1999).
[23] V. P. Glazkov and I. N. Goncharenko, Fiz. Tekh. Vysokih Davlenij **1**, 56 (1991) (in Russian).
[24] J. Rodríguez-Carvajal, Physica B **192**, 55 (1993).
[25] K. K. Pandey, H. K. Poswal, R. Kumar, and S. M. Sharma, J. Phys.: Condens. Matter **25**, 325401 (2013).
[26] F. J. Birch, J. Geophys. Res. **91**, 4949 (1986).
[27] A. Grzechnik, M. Tolkiehn, W. Morgenroth, and K. Friese, J. Phys.: Condens. Matter **22**, 275401 (2010).
[28] D. L. Rousseau, R. P. Bauman, and S. P. S. Porto, J. Raman Spectrosc. **10**, 253 (1981).
[29] B. Mihailova, M. M. Gospodinov, B. Güttler, F. Yen, A. P. Litvinchuk, and M. N. Iliev, Phys. Rev. B **71**, 172301 (2005).
[30] M. N. Iliev, M. V. Abrashev, H.-G. Lee, V. N. Popov, Y. Y. Sun, C. Thomsen, R. L. Meng, and C. W. Chu, Phys. Rev. B **57**, 2872 (1998).
[31] M. N. Iliev, H.-G. Lee, V. N. Popov, M. V. Abrashev, A. Hamed, R. L. Meng, and C. W. Chu, Phys. Rev. B **56**, 2488 (1997).
[32] A. Congeduti, P. Postorino, E. Caramagno, M. Nardone, A. Kumar, and D. D. Sarma, Phys. Rev. Lett. **86**, 1251 (2001).
[33] D. P. Kozlenko, L. S. Dubrovinsky, I. N. Goncharenko, B. N. Savenko, V. I. Voronin, E. A. Kiselev, and N. V. Proskurnina, Phys. Rev. B **75**, 104408 (2007).
[34] A. Muñoz, J. A. Alonso, M. T. Casais, M. J. Martínez-Lope, J. L. Martínez, and M. T. Fernández-Díaz, Phys. Rev. B **65**, 144423 (2002).
[35] R. D. Shannon, Acta Crystallogr. A **32**, 751 (1972).
[36] J. W. Kim, S. Y. Haam, Y. S. Oh, S. Park, S.-W. Cheong, P. A. Sharma, M. Jaime, N. Harrison, J. H. Han, G.-S. Jeon, P. Coleman, and K. H. Kim, Proc. Natl. Acad. Sci. USA **106**, 15573 (2009).
[37] R. P. Chaudhury, C. R. dela Cruz, B. Lorenz, Y. Sun, C.-W. Chu, S. Park, and S.-W. Cheong, Phys. Rev. B **77**, 220104(R) (2008).